Jour. Fac. Sci., Hokkaido Univ., Ser. VII (Geophysics), Vol. 11, No. 2, 501-521, 1998.

The Basin Expansion Mechanism of a Supraglacial Lake in the Nepal Himalaya

Kazuhisa Chikita

Division of Earth and Planetary Sciences, Graduate School of Science, Hokkaido University, Sapporo 060-0810, Japan

Jageshwar Jha

Water and Energy Commission Secretariat, Ministry of Water Resources, P.O. Box 1340, Singha Darbar, Kathmandu, Nepal

and

Tomomi Yamada

Institute of Low Temperature Science, Hokkaido University, Sapporo 060-0819, Japan

(Received November 30, 1997)

Abstract

The mechanism on the basin expansion of a supraglacial lake in the Nepal Himalaya is developed by examining thermal and hydrodynamic conditions. Supraglacial Tsho Rolpa Lake (27°51'N, 86°29'E ; water level, 4580 m asl ; surface area, 1.39 km^2 in 1994) has increased the size on the tongue of debris-covered Trakarding Glacier since late 1950s (surface area, 0.23 km^2 in 1958). The lake-basin expansion occurs in combination of the bottom subsidence from the ice melt below the lake bottom and a horizontal retreat of the glacier terminus. The lake is pycnally stratified by suspended sediment concentration (SSC) of water rather than water temperature. The observations in the premonsoon of 1996 revealed that a great retreat of the glacier terminus results from the increased ice melt at the subaqueous lower part by a direct contact of relatively warm surface water ($>\sim$5°C) and the consequent calving at the aerial upper part. The warm surface water is transported toward the glacier terminus by wind-driven currents, which are generated by a diurnal valley wind. Sediment-laden underflows are produced by glacier-melt sediment discharge from a subaqueous tunnel mouth at the glacier terminus. The downslope movement of the underflows probably causes the turbulent heat diffusion up to near the deepest point. Thermal conditions on the lake bottom (less than about 30 m in depth) near the end moraine vary diurnally by the oscillation of the thermocline or metalimnion. The bottom thermal conditions at more than 30 m in depth are nearly constant or constant to the side of the end moraine, suggesting the relatively weak or nearly molecular heat diffusion.

1. Introduction

Some of debris-covered glaciers in the Nepal Himalaya have supraglacial lakes on the tongues. These lakes have expanded increasingly since late 1950s. Tsho Rolpa Lake in the Rolwaling Valley, Eastern Nepal is one of such supraglacial lakes increasing the size, and is now in danger of outburst (Yamada, 1993). The lake has expanded horizontally by the retreat of the glacier terminus (the Trakarding Glacier or the lower Trambau Glacier) and vertically by the bottom subsidence due to the dead ice melt below the bottom. The lake (about 3,000 m long and 410 to 630 m wide in 1994) is at present dammed up completely by the end moraine and part of the lateral moraine. Topographical, hydrological and thermal conditions of the lake have been investigated by Mool et al. (1993), Kadota (1994), Sakai (1995), Yamada (1996), Chikita et al. (1996b) and Chikita et al. (1997). In this study, we will emphasize systematic relations between the lake basin expansion and lake-current dynamics, using some data sets obtained in the premonsoon of 1996.

2. Study area and methods

Supraglacial Tsho Rolpa Lake (27°51'N, 86°29'E) is located at 4,580 m above sea level in the Himalayan region of the Tama Kosi River, Eastern Nepal (see Fig. 1), and is in contact with the cliff-shaped terminus of debris-covered

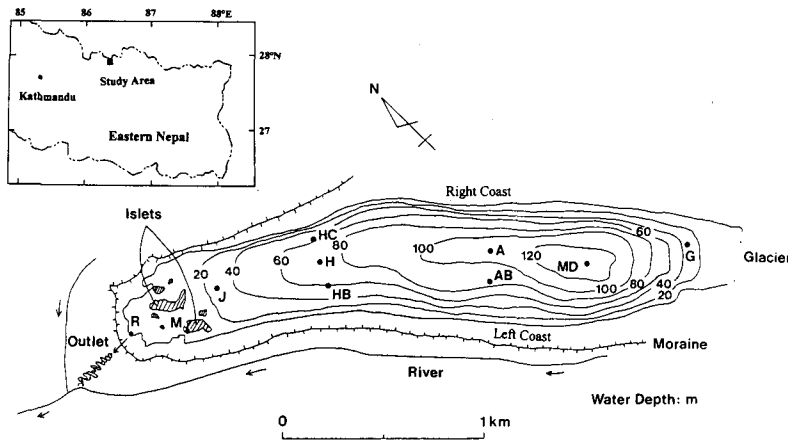

Fig. 1. Locations of supraglacial Tsho Rolpa Lake in the Eastern Nepal and observation sites on the bathymetric map (partially modified after Kadota, 1994).

Trakarding Glacier. The drainage basin including the lake is 77.6 km^2 in area (Sakai, 1995), geologically consisting of Precambrian sedimentary and metamorphic rocks and volcanic intrusion of various periods. The maximum and mean depths are 131 m and 55.1 m, respectively in 1994. The lake is developed on the Trakarding Glacier tongue, and is bordered by the lateral moraine with the steep slope (25-80°) and the end moraine partially including the fossil ice. The uplake end directly contacts with the cliff-shaped glacier terminus. The outer slope (angle, 8.5-16.7°) of the end moraine is about 150 m high. There is a bottom channel about 30 m wide extending from a tunnel mouth at the glacier terminus. This was probably built up from the selective glacier-melt by meltwater discharge from the tunnel mouth (Yamada, 1996).

A field survey in the lake was carried out from 27 May to 9 June 1996 during the premonsoon season. Figure 1 shows the site locations for observation on the bathymetric map. Sites J, H, A and MD are located along the thalweg of the elongated lake basin. Site G is situated about 260 m off the glacier terminus. At all the sites in Fig. 1, vertical measurements (every 0.2 m in depth) of water temperature and turbidity were made by lowering a sonde of 500 m water proof (TCTD Profiler : model ASTB200-P-64K, Alec Electronics Co., Ltd.) with

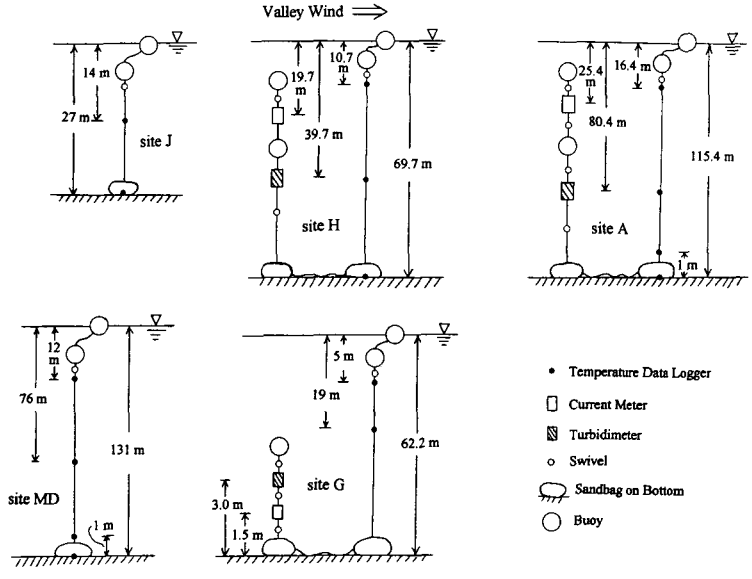

Fig. 2. Sandbag-buoy-swivel systems for mooring current meters, turbidimeters and temperature data loggers at sites J, H, A, MD and G.

a water pressure gauge (range of 0-200 m, accuracy of ±0.3% FS), a platinum thermometer (accuracy of ±0.05°C) and a turbidity sensor (accuracy of ±0.04 g/L) of infrared ray back-scattering type. At site G, vertical profiles were obtained just out of the bottom channel (43.4 m in depth). Turbidity values from the TCTD Profiler were converted into suspended sediment concentration (SSC; g/L) of water, by using significant correlation ($r=0.94$) between turbidity and SSC of lake water sampled simultaneously.

Meantime, at sites G, MD, A, H and J, we continuously measured water temperature with temperature data loggers, and at sites G, A and H, also flow velocity and water turbidity with self-recording electromagnetic current meters and turbidimeters, respectively. The current meter with a thermistor sensor (accuracy of ±0.5 cm/s for horizontal current speed, ±3° for horizontal current direction, and ±0.1°C for temperature), the turbidimeter (accuracy of ±0.04 g/L) and two to four temperature data loggers (accuracy of ±0.15°C or ±0.2°C) were fixed by using mooring sandbag-buoy-swivel systems (Fig. 2). At site G, the mooring system was fixed in the bottom channel (62.2 m in depth), extending from the glacier terminus. The turbidity from self-recording turbidimeters was likewise converted into SSC because of the same turbidity sensor as that of the TCTD Profiler. The flow velocity, turbidity and water

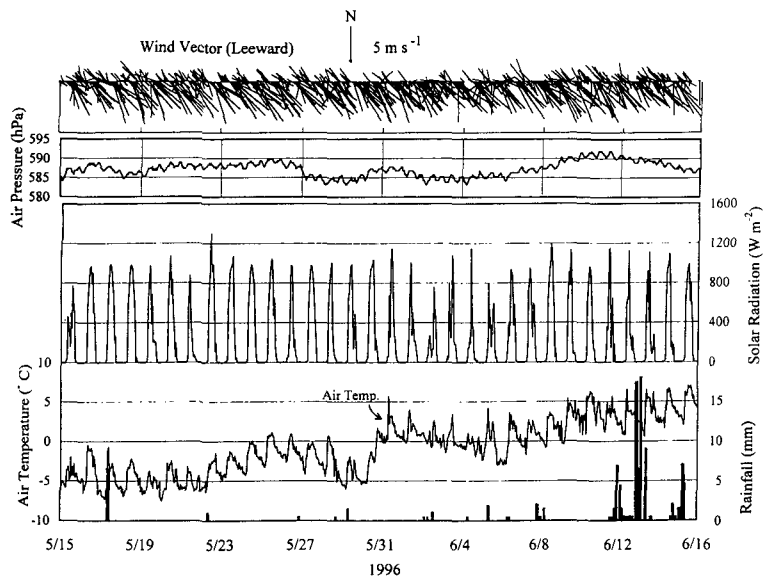

Fig. 3. Meteorological conditions observed every 1 hr at site M for 15 May-15 June 1997.

temperature were recorded at 10 min or 15 min intervals.

Lake water level and water discharge at an outlet (site R in Fig. 1) and meteorology at site M have been recorded every 1 hour since June 1993 by Water and Energy Commission Secretariat (WECS), Ministry of Water Resources, Nepal. Hydrological conditions of the lake are detailed by Yamada (1996).

3. Results

3.1 Meteorological conditions

Figure 3 shows time series of meteorological data recorded at site M for a period 15 May to 15 June 1996. Before 31 May, air temperature kept around 0°C or less, showing that it was much colder than in the same period of 1995 (Chikita et al., 1997). The continual heavy rainfalls since 11 June typifies the opening of the monsoon season of 1996. Wind speed, air temperature and solar radiation exhibit clear diurnal variations. The daytime rainfall of 2 and 5 June considerably decreased the solar radiation. Except the two days, the solar radiation gave the stable heat supply for the lake warming. Most of the radiative heat could be absorbed at the lake surface because of the low albedo ($<\sim 0.05$ on the daytime). The sensible heat is responsible for cooling the lake, because the lake surface keeps about 5°C or more. The water temperature is higher than air temperature except on the daytime of 31 May.

A weak mountain (southeast to south-southeast) wind blew typically at less than 1 m/s during the increased air pressure at 3 : 00-8 : 00, while a relatively strong valley (northwest to north-northwest) wind prevailed at 2-7 m/s during the decreased pressure at 10 : 00-19 : 00. Both the winds thus prevailed in the longitudinal direction over the lake (see Fig. 1). The valley wind is possibly due to the upslope air advection of large scale in the Himalaya. It should be noted that the strong valley wind blows toward the glacier terminus which contacts directly with the lake water. This wind may produce wind waves at the lake surface and wind-driven currents in the surface layer. Taking the water depths into account, the wind waves could be deep water gravity waves which are negligible for the mass or heat transport. The waves would produce some glacier-melt near the lake surface, only when they collide with the glacier terminus. The wind-driven currents are likely to effectively transport the absorbed radiative heat toward the glacier terminus because of the long fetch (about 3 km) for the valley wind. The wind-driven currents could thus be very responsible for melting subaqueous part of the glacier terminus, by putting relatively warm surface water in contact with the glacier terminus.

3.2 *Spatial distribution of water temperature, SSC and water density*

Figures 4 and 5 show longitudinal distributions of water temperature, suspended sediment concentration (SSC) and water density *in situ*, σ based on the temperature and turbidity data of the TCTD profiler. These were obtained on the morning (8 : 35-10 : 19) (Fig. 4) and on the afternoon (15 : 44-17 : 08) (Fig. 5) of 2 June 1996. Here σ is defined by the following equations :

$$\sigma=(\rho_{TC}-1{,}000)\times 10 \tag{1}$$

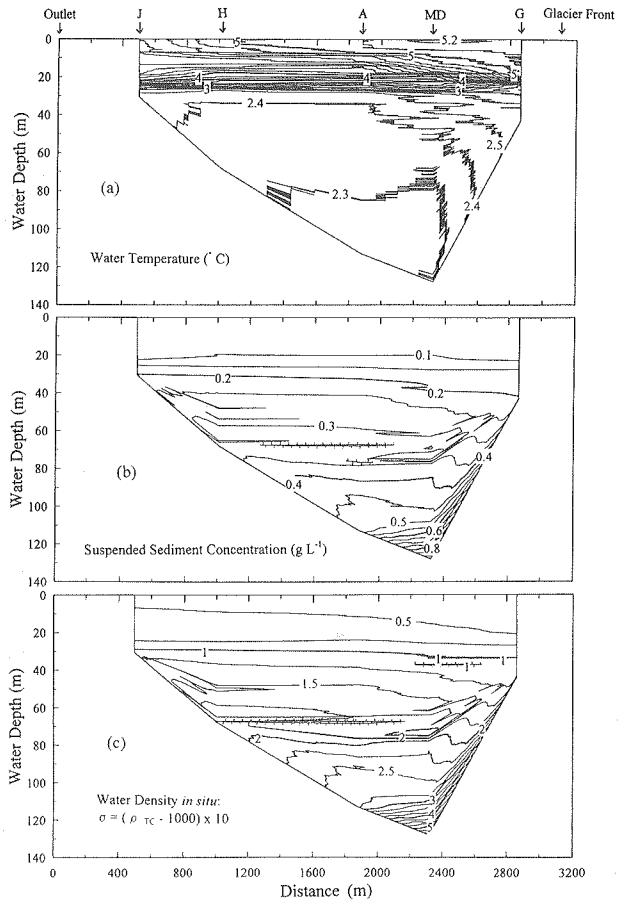

Fig. 4. Longitudinal distributions of (a) water temperature, (b) SSC and (c) water density *in situ*, σ, obtained by the TCTD Profiler at 8 : 35-10 : 19 on 2 June 1996. Isopleth interval : (a) 0.1°C, (b) 0.05 g/L and (c) 0.25.

$$\rho_{TC} = (1 - C/\rho_S)\rho_T + C \tag{2}$$

where ρ_{TC} is the water density in kg/m^3 with suspended sediment concentration, C (g/L) at temperature, T (°C), ρ_S is the density of suspended sediment (=2650 kg/m^3 for Tsho Rolpa sediment ; Sakai, 1995), and ρ_T is the pure water density at T. Dissolved solids in lake water were here neglected because of less than 0.001 g/L, thus being much less than the observed lowest SSC (0.05 g/L).

A comparison between Figs. 4 and 5 allows us to recognize temporal changes of thermal, SSC and density structures for about 7 hrs. The time

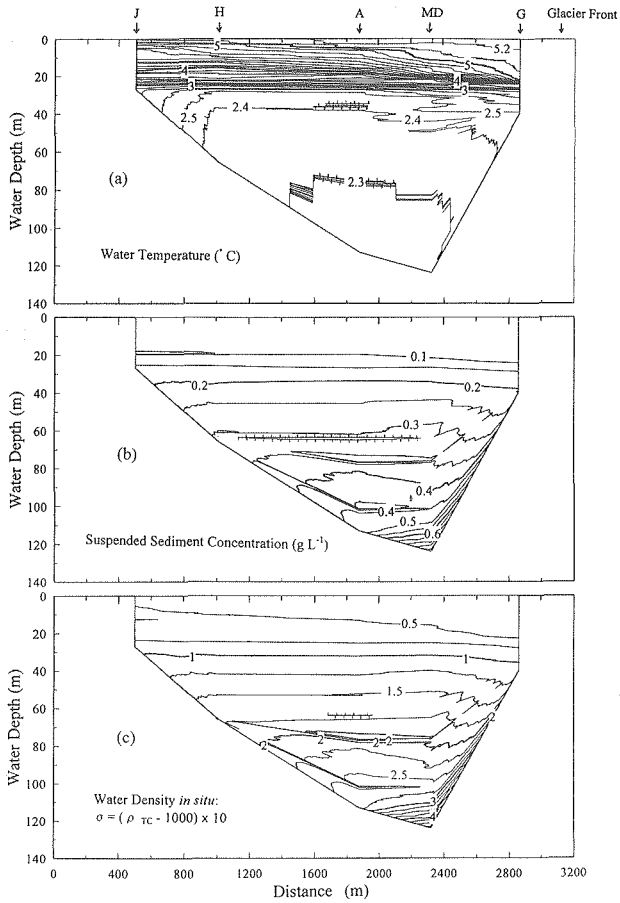

Fig. 5. Longitudinal distributions of (a) water temperature, (b) SSC and (c) water density *in situ*, σ, obtained by the TCTD Profiler at 15 : 44-17 : 08 on 2 June 1996. Isopleth interval : same as in Fig. 4.

period of 8 : 35-10 : 19 corresponds to the early stage of time when the lake surface starts to absorb the solar radiation and a valley wind starts to blow, while that of 15 : 44-17 : 08 is equivalent to the late time for the solar radiation and valley wind. The weak pycnocline lay at about 27 m in depth at any time (see the isopleths of $\sigma=0.75$ and 1 in Figs. 4c and 5c), while the metalimnion existed at depths of 15 m-28 m with the thermocline (point of the greatest temperature gradient in the metalimnion) at about 25 m (Figs. 4a and 5a). A quasi-isopycnal layer above the pycnocline was probably produced through turbulent mixing by the valley wind. Meantime, in the mixed layer the wind generated the horizontal gradients of water temperature (see the isotherms of 4.6-5.1°C) and σ (see the isopleth of 0.5) toward the glacier front (or terminus), irrespective of no gradient in SSC. This indicates that in the mixed layer, σ depends on water temperature rather than SSC because of the low SSC at 0.15 g/L or less. As noted by the isotherm of 5°C or more, in the afternoon, the warm water zone in the surface layer extended toward downlake, and the temperature gradient increased toward the glacier terminus, especially between sites MD and G. This means the heat transport toward the glacier terminus and the consequent net heat storage in front of the glacier terminus, by means of *wind-driven currents* from the valley wind. The wind-driven currents could thus exalt the ice-melt at the underwater part of the glacier terminus and the consequent *calving* of the upper aerial part (Chikita et al., 1997). Cold lake water at less than 5°C produced by the glacier contact would plunge in front of the glacial cliff and then move downlake near the pycnocline as *countercurrents* compensating for the upper wind-driven currents. The *vertical water circulation* is thus possibly produced in the mixed layer above the pycnocline.

Below the pycnocline, the distribution patterns of SSC are similar to those of σ. It is thus seen that the water density depends on SSC rather than temperature. The high SSC zone (0.5 g/L or more) near the bottom from site G through site A suggests that *sediment-laden underflows* occur in front of the glacier terminus, due to the ice-melt sediment discharge from a mouth of englacial tunnels, and then go downslope to the deepest zone (Chikita et al., 1997; Yamada, 1996). Assuming that the upper interface of the underflows corresponds to the isopleth of 0.5 g/L, the flow thickness is about 21-24 m at site MD (Figs. 4b and 5b). Suspended sediment transported by the underflows is mostly silt and clay of 0.7-15.6 μm in diameter (Yamada, 1996). The slow settling velocity of 2.6×10^{-7}-1.3×10^{-4} m/s could cause some stagnation of suspension and thus strong stratification near the bottom. Sediment-laden underflows tend to transport relatively cold water because of its generation from ice-melt water

discharge. The cold zone (<2.3°C) at depths of more than 80 m is thus continued by the stagnation of suspension supplied by the underflows.

There are many isoplethic peaks of temperature at 2.4 and 2.5°C at depths of 30-60 m between sites G and A. In Fig. 4a, these relatively warm peaks appear to horizontally move from near the glacier front and, in Fig. 5a, to reach to depths of 30-60 m at sites H and J. The relatively warm zone of 2.4-2.5°C near site G could be formed by the mixing between the warmest surface water (~5°C) and inflowing ice-melt water (~0°C). The horizontal movement is considered to have occurred as part of countercurrents through a vertical momentum transfer which resulted from the weak density stratification at depths of less than 60 m (see Figs. 4c and 5c). By comparison between Figs. 4a and 5a, the average speed of the horizontal currents is estimated at about 0.05 m/s.

Spikelike isoplethic peaks of SSC (0.25 g/L to 0.35 g/L) or σ (1.25 to 1.75) between sites G and MD suggest that the water at about 50 m and 60 m in depth plunges into the relatively turbid or heavy deeper zone and then intrudes horizontally at 65 m and 75 m of site MD, respectively (see Figs. 4b, 4c, 5b and 5c). These currents have the relatively low speed at about 0.02 m/s. The plungings probably indicate the movement of downward *compensation currents* in the weakly stratified zone which are initiated from the entrainment at the upper interface of sediment-laden underflows. Some local minimums on the vertical SSC profiles reported by Yamada (1996) were probably built up by these relatively clear currents intruding at some depths. As shown by the isopleths of C=0.4 g/L and σ=2.5 in Figs. 5b and c, the relatively low SSC (or σ) zone appeared at a depth of about 100 m at downlake from site MD. This unstable condition was probably produced also by the downward compensation currents and their subsequent *intrusion* (*intruding currents*).

The above currents shown by temperature or SSC (or σ) isopleths thus do not correspond to density interflows driven only by the pressure gradient between the source and frontal snout of the flows (for behaviors of interflows, e. g., see Hamblin and Carmack, 1978).

The effect of *Coriolis deflection* on the movement of the countercurrents or intruding currents is estimated by the Rossby number $Ro = U/fL$, where U is the flow speed, f is the Coriolis parameter, and L is the lateral basin scale at the depth where the currents intrude. The Coriolis deflection is not completely neglected for the Tsho Rolpa currents, since $Ro = 1.0 \sim 1.5$, giving $f = 6.81 \times 10^{-5}$ rad/s, $U = 0.02$-0.05 m/s and $L = 300$-500 m.

Figures 6 and 7 show distributions of temperature, SSC and σ in the

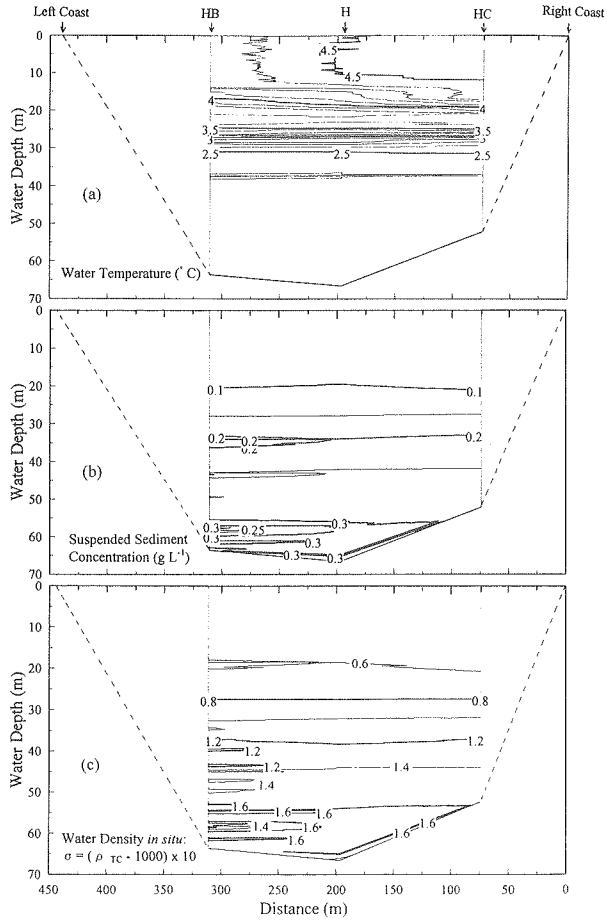

Fig. 6. Distributions of water temperature, SSC and water density *in situ*, σ in the transverse section of sites HC, H and HB, observed at 7 : 22–7 : 49 on 6 June 1996. Isopleth interval : (a) 0.1°C, (b) 0.05 g/L and (c) 0.2.

transverse section along sites HC, H and HB at 7 : 22–7 : 49 on 6 June and along sites A and AB at 7 : 15–7 : 37 on 5 June, respectively. At these early times, the lake surface did not yet receive the solar radiation. At depths less than about 15 m, relatively warm water at more than 4.5°C is biased on the right side. This is probably due to the relatively strong mixing in the surface layer by a valley wind centered on the right side on the previous days (4 and 5 June). At depths more than 55 m, as shown by the isopleths of $C=0.3$ g/L and $\sigma=1.6$, the water of relatively large SSC and σ lies on the right side. This is probably caused by

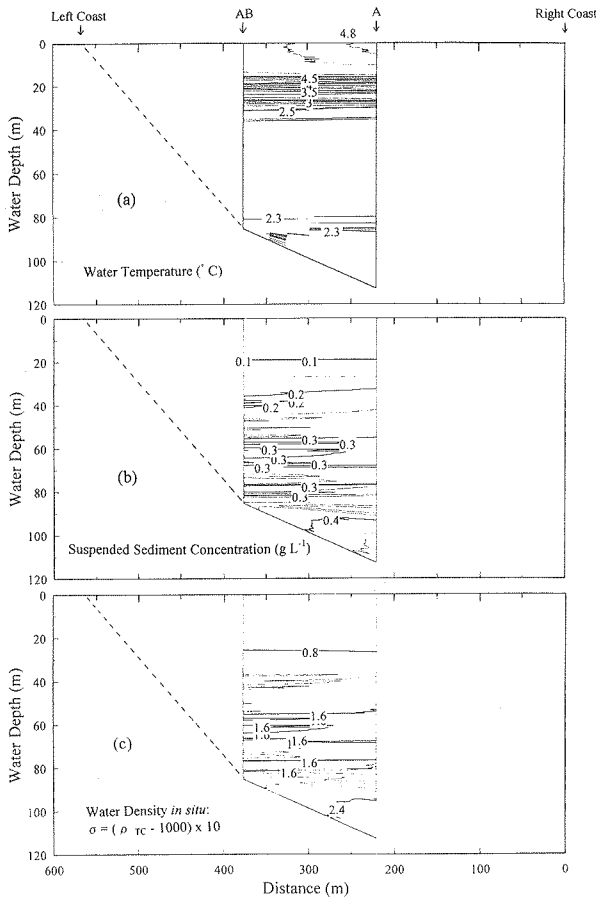

Fig. 7. Distributions of water temperature, SSC and water density *in situ*, σ in the transverse section of sites A and AB, observed at 7 : 15-7 : 37 on 5 June 1996. Isopleth interval : (a) 0.1°C, (b) 0.05 g/L and (c) 0.4.

the position of turbid meltwater inflow at the glacier terminus biased to the right (see Fig. 1).

3.3 Continuous measurement of flow velocity, water temperature and SSC

As shown by Figs. 4 and 5, the density structure of the lake above the pycnocline (about 27 m in depth) is controlled by water temperature, where SSC is about 0.15 g/L or less. Below the pycnocline, however, the water density is rather dominated by SSC as SSC increases with increasing depth, especially near the bottom. Near the pycnocline, the lake exhibits a marked change in

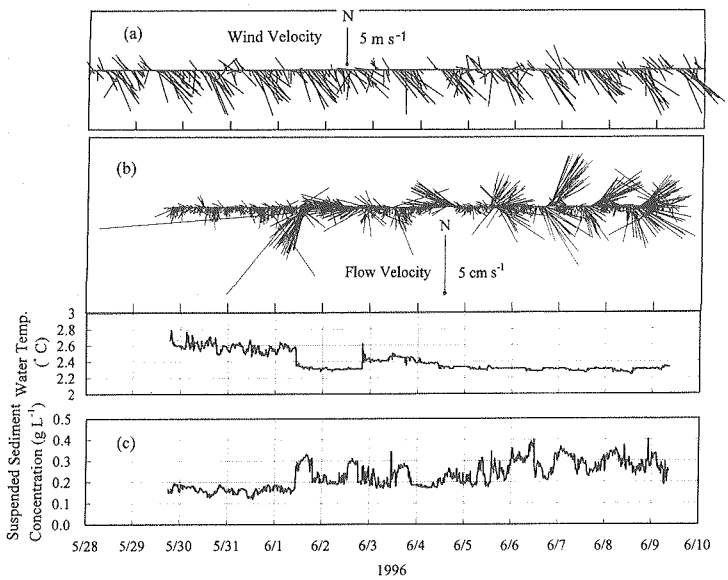

Fig. 8. Time series of (a) wind velocity at site M, (b) flow velocity and water temperature recorded at 1.5 m above the bottom at site G, and suspended sediment concentration at 3 m above the bottom at site G. (a), (b) and (c) are described by the data obtained at 1 hr, 10 min and 15 min intervals, respectively.

temperature rather than in SSC. Continuous temperature records near the pycnocline could thus exhibit water motions characteristic of the wind-built setup or internal free oscillations such as internal seiche ; continuous SSC and temperature records near the pycnocline or below probably shows temporal variations based on dynamic behaviors of downward compensation currents, their intrusion or sediment-laden underflows.

Figure 8 shows time series of (a) wind velocity at site M, (b) flow velocity and water temperature at 1.5 m above the bottom (60.7 m depth) at site G, and (c) SSC at 3 m above the bottom (59.2 m depth) at site G (see Fig. 2). The records in Figs. 8b and 8c could indicate dynamic behaviors of the glacier-melt water discharge from a subaqueous tunnel mouth at the glacier terminus. As shown by the meteorological conditions in Fig. 3, air temperature abruptly increased at more than 0°C on 31 May, and then gradually decreased until 4 June almost at less than 0°C. The water temperature and SSC records show that with response to the gradual decrease of air temperature at more than 0°C, glacier-melt sediment discharge diurnally occurred for 1-4 June with a gradual decrease of the SSC. The maximum SSC during the sediment discharge

appeared at 15 : 30-16 : 15 with a time lag of 27-28 hrs for air temperature. The glacier-melt discharge thus appears to be sensitive to the sensible heat rather than the solar radiation. This is possibly due to the thick debris cover on the ablated Trakarding Glacier. The cold condition on 4 June probably induced irregular variations of SSC on 5 June. Thereafter, an increase of air temperature at more 0°C on the daytime of 5-7 June raised the sediment discharge with relatively high SSC for 6-8 June with a time lag of 6.5-14 hrs. The water discharge during the high SSC, however, was probably small, because the flow velocity kept small at 0.9-2 cm/s south-southwestward to northwestward (i.e., downslope direction on the bottom of site G). The relatively rapid response of SSC to air temperature suggests that the small sediment discharge was produced by melting probably in the relatively downstream region of the glacier.

The water temperature keeps 2.3-2.5°C since 1 June. The inflowing meltwater probably has the temperature of 0°C because of the discharging through en-glacial tunnels. The temperature records at site G thus suggest the consequence of mixing with the warm water at about 5°C (see Figs. 4a and 5a).

The flow velocity records in Fig. 8b indicate that corresponding to the high SSC on 1-4 June, lake currents were strengthened in the southwest to northwest directions, thus in the downslope direction at site G (see Fig. 1). This suggests that sediment-laden underflows were produced by the glacier-melt sediment discharge. The underflows are driven by the product of downslope buoyant gravity and layer thickness (Chikita et al., 1991, 1996a). During the low and increasing SSC for 5-9 June, flow velocity kept high at 2-6 cm/s south-southeastward to east-southeastward and northeastward to north-northeastward, respectively. These currents thus have the vector component directed to the glacier terminus. The strong currents then changed their directions in response to the wind directions in Fig. 8a. This suggests that a vertical momentum transfer by the countercurrents in the vertical water circulation occurred down to near the bottom of site G. In fact, as shown by isopleths of $\sigma = 1.25$ to 1.75 in the density structure of 5 June (Fig. 9), the density stratification was weakened at depths of 40-60 m between sites G and MD (cf. Figs. 4c and 5c). During the observation time of 7 : 35-10 : 41 on 5 June, the flow velocity (or water discharge) was small, though the SSC was relatively high at 0.23-0.31 g/L (see Fig. 8b). The consequent small sediment discharge probably generated the stratification decline and the deepening of vertical momentum transfer. This condition was possibly continued for 5-8 June with extending the relatively clear zone at uplake of site MD (Fig. 9b).

Figure 10 shows time series of (a) wind velocity at site M and (b) flow

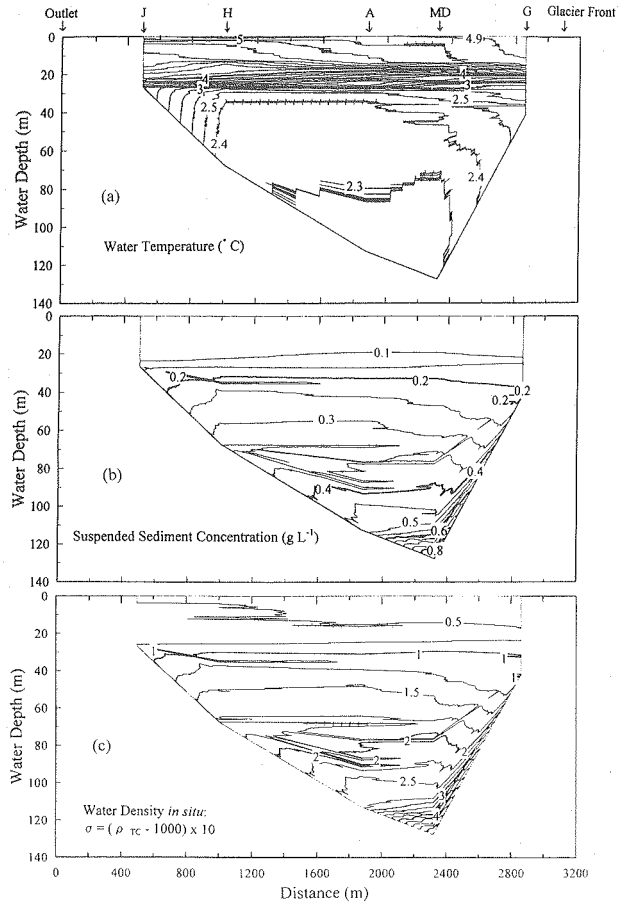

Fig. 9. Longitudinal distributions of (a) water temperature, (b) SSC and (c) water density *in situ*, σ, obtained by the TCTD Profiler at 7 : 35-10 : 41 on 5 June 1996. Isopleth interval : same as in Figs. 4 and 5.

velocity and water temperature at a depth of 25.4 m at site A. The thermocline and pycnocline at site A was then located at about 25 m and 27 m in depth, respectively (Figs. 4a and 5a). It is evident that current vectors respond in opposite directions to wind velocity. During the valley wind, water temperature decreased with increasing flow speed. These indicate that in order to compensate for wind-driven currents in the upper layer, countercurrents occurred near the thermocline or pycnocline, and that the strengthened setup induced the lift of the lower cold water. A combination of the wind-driven currents and countercurrents thus establishes a current system of vertical water circulation

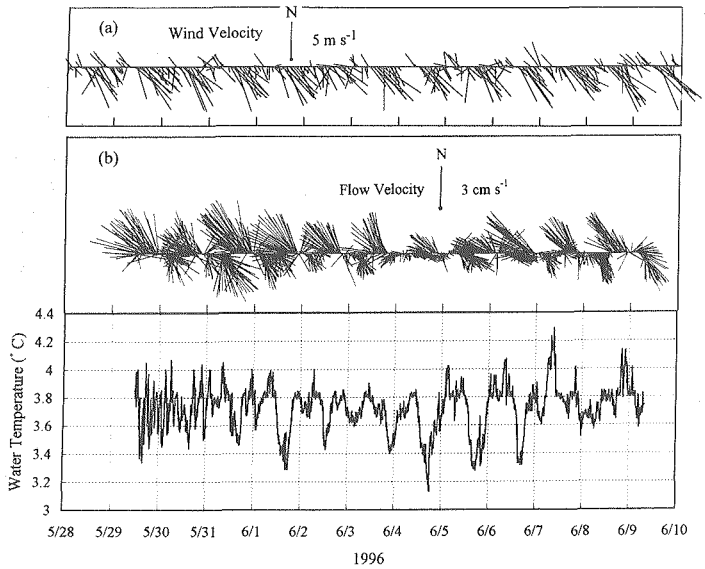

Fig. 10. Time series of (a) wind velocity at 1 hr intervals at site M, (b) flow velocity and water temperature recorded every 10 min at a depth of 25.4 m at site A.

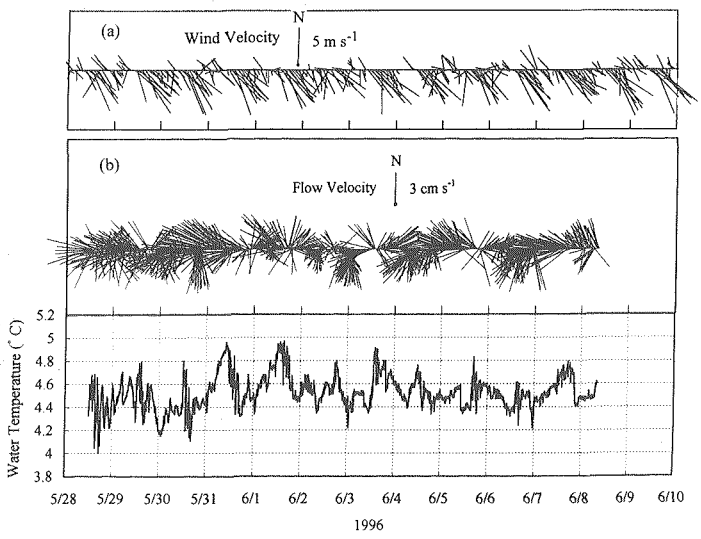

Fig. 11. Time series of (a) wind velocity at 1 hr intervals at site M, (b) flow velocity and water temperature recorded every 10 min at a depth of 19.7 m at site H.

in the quasi-isopycnal mixed layer during the leeward setup.

Continuous records of flow velocity and water temperature at 19.7 m in depth of site H (Fig. 11) showed that during the valley wind, the flow velocity changed westward to north-northwestward with increasing water temperature (e.g., see the variation on the morning of 31 May), but with decreasing temperature, west-southwestward to southwestward (e.g., see the variation on the afternoon of 31 May) or northward to northeastward (e.g., see the variations on the afternoon of 1 and 3 June). The flow speed was then sensitive to the wind speed except during the weak mountain wind. The longitudinal downlake direction at site H is west-northwestward or northwestward (see Fig. 1). This means that countercurrents at site H probably appeared during the increase of water temperature. The temperature increase is likely caused by the radiative heat absorption at the surface and its downward turbulent diffusion by wind mixing, since at comparable wind speeds, the diurnal maximum water temperatures appear to respond to the maximum solar radiations (Fig. 3). The subsequent temperature decrease is probably due to the lift of the lower cold water accompanying the developed setup or to the nocturnal cooling by a sensible heat transfer. The west-southwestward to southwestward (or northward to northeastward) flow during the setup then occurred probably as part of countercurrents (or part of wind-driven currents). The measurement depth (19.7 m) at site

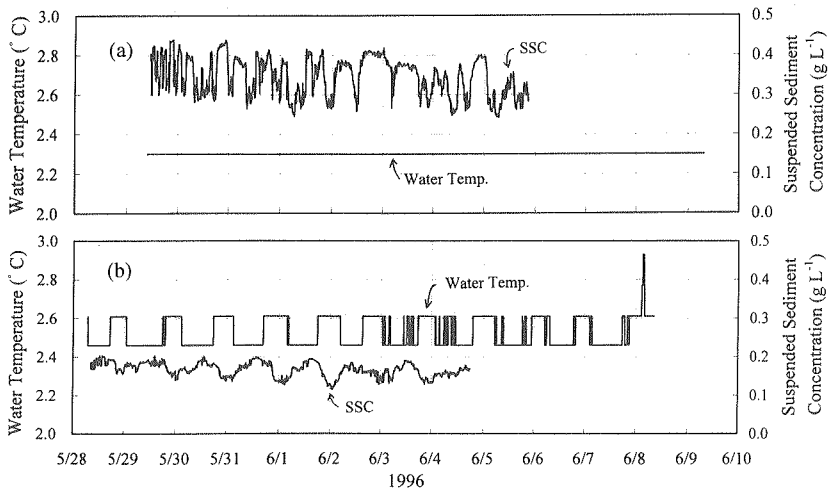

Fig. 12. Time series of water temperature and suspended sediment concentration (SSC) recorded at 10 min intervals (a) at a depth of 80.4 m at site A and (b) at a depth of 39.7 m at site H.

H thus corresponds to a point with some sensitivity to solar radiation, air temperature and wind.

Figure 12 shows temperature and SSC records at (a) 80.4 m of site A and at (b) 39.7 m of site H. The depth of site H is located in the relatively turbid zone below the metalimnion (Figs. 4 and 5), and thus the amplitude (0.16°C) of the temperature variation is smaller than that near the thermocline at site A (Fig. 10b). As the valley wind is strengthened in the morning, at site H the temperature decreases and the SSC increases. This means that the uplift of relatively cold and turbid water diurnally occurs by the leeward setup toward the glacier terminus. This diurnal oscillation is evidenced by the FFT (Fast Fourier Transform) spectral analysis of the SSC data at site H (Fig. 13).

Meantime, the 80.4 m records at site A exhibit non-variation in temperature and higher frequency in SSC (Fig. 12a). The FFT spectral analysis revealed that SSC at sites A and G oscillates with relatively short periods of 6 hrs, 4 hrs and 2 hrs rather than 24 hrs at site H (Fig. 13). Hence, the water motion at site A is not related to the diurnal vertical water circulation, but to intruding currents starting at near site MD (see Figs. 4b and 5b) or their surrounding water motions, since the intruding currents could be generated by the downward compensation currents connected to the entrainment by sediment-laden underflows. The constant temperature (2.30°C) at 80.4 m of site A suggests the

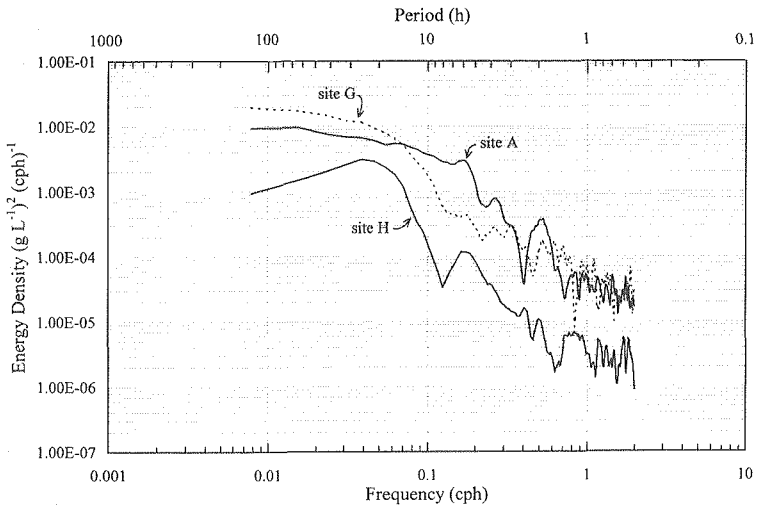

Fig. 13. FFT power spectra of SSC (g/L) for 10 : 15 30 May-18 : 00 4 June at 3 m above the bottom at site G, at a depth of 80.4 m at site A and at a depth of 39.7 m at site H.

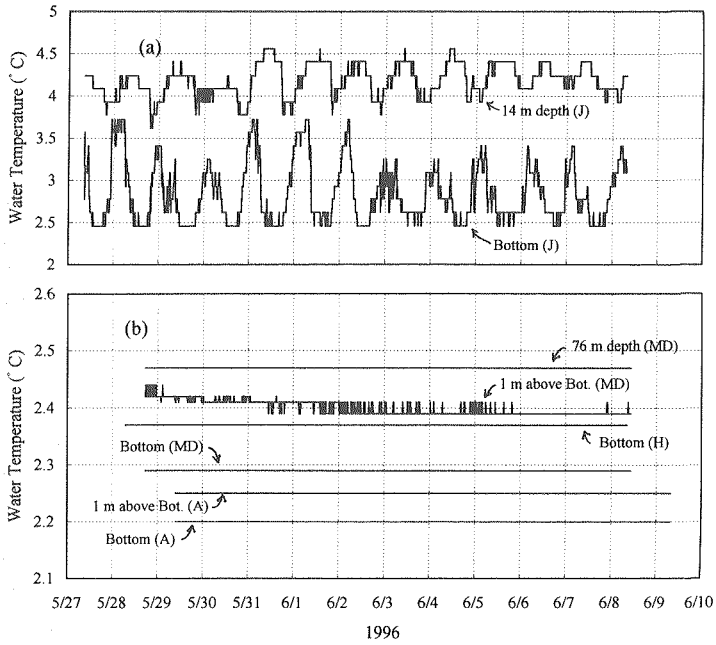

Fig. 14. Time series of water temperature at 10 min intervals (a) at depths of 14.0 m and 27.0 m (bottom) at site J, and (b) at a depth of 69.7 m (bottom) at site H, at depths of 114.4 m (1 m above the bottom) and 115.4 m (bottom) at site A and at depths of 76.0 m, 130 m (1 m above the bottom) and 131 m (bottom) at site MD.

continual supply of suspension water transported by the intruding currents probably with SSC of more or less 0.35 g/L.

Water temperature at a depth of 114.4 m (1 m above the bottom) at site A and at a depth of 76 m at site MD also kept constant at 2.25°C and 2.47°C, respectively (Fig. 14). The water supply by intruding currents is thus likely to continue in the deep zone. With increasing valley-wind velocity in the morning, water temperature at 27 m depth (bottom) of site J decreased more greatly than that at 14 m with a time lag of about 3 hrs (Fig. 14a). This is because the leeward setup makes the thermocline lift in the downlake region of site MD, and also the 27 m depth is relatively near from the thermocline (see Figs. 4a and 5a). The vertical water circulation system is thus likely to prevail longitudinally in the quasi-isopycnal mixed layer. Hence, a thermal condition on the bottom, related to the fossil-ice melt near the end moraine, is unsteady by the metalimnion (2.5-4.5°C) oscillation accompanying the leeward setup and the simultaneous vertical circulation.

At 130 m depth (1 m above the bottom) of site MD, a slight variation in temperature is seen with a range of 2.39-2.44°C (Fig. 14b). As noted by the isopleth of 2.3°C in Figs. 4a, 5a and 9a, the temperature near the bottom of site MD varies temporarily in spite of the interior of sediment-laden underflows. This indicates that sediment-laden underflows have unsteady and non-uniform vertical temperature. Hence, the temperature variation in Fig. 14b suggests a weak water motion by sediment-laden underflows which reached to the deepest zone. In fact, the isopleths of $C>=0.5$ g/L in Figs. 4b and 5b, indicating behaviors of the underflows, exhibit different distribution patterns. The bottom temperature at sites MD, A and H remains constant at 2.29°C, 2.20°C and 2.37°C, respectively, and thus a water motion near the bottom appears to be negligible or, if any, very weak. Hence, the bottom thermal conditions are probably controlled by nearly molecular or weak heat diffusion.

Conclusions

Vertical and continuous measurements of water temperature and SSC revealed that dynamic behaviors of lake currents such as wind-driven currents, countercurrents, compensation currents, intruding currents and sediment-laden underflows dominate the internal thermal structure of supraglacial Tsho Rolpa Lake. Findings on their contribution to the lake expansion are as follows:

(1) The lake has the very clear thermocline (3 or 4°C or around) at about 25 m in depth irrespective of the weak pycnocline. This is because the water density structure is controlled by the amount of fine suspended sediment supplied by glacier-melt discharge from a tunnel mouth at the glacier terminus. In the surface layer, wind-driven currents dominate the advective diffusion of heat, especially the radiative heat absorbed at the surface, while cold meltwater of relatively high turbidity is spread in the deeper zone by part of countercurrents, downward compensation currents, intruding currents and sediment-laden underflows. The vertical water circulation, composed of wind-driven currents and countercurrents, is accompanied by diurnal oscillations of the thermocline or metalimnion. The oscillations could greatly affect the thermal conditions on the lake bottom near the end moraine.

(2) In the mixed layer, wind-driven currents from the valley wind transport the absorbed heat up to the glacier terminus. The consequent setup and vertical water circulation make relatively warm water of $>\sim$5°C in direct contact with the glacier ice. This could exalt the ice-melt at the lower part of the glacier terminus and induce the calving of the upper part. This is a scenario

for the horizontal, large lake expansion or great glacier retreat.

(3) Because of the weak density stratification at the pycnocline, the countercurrents compensating for the upper wind-driven currents could conduct a vertical momentum transfer below the pycnocline. As a result, the horizontal currents are initiated as part of countercurrents from the mixing zone near the glacier terminus. The currents could affect bottom thermal conditions at a range of 40-60 m in depth by reaching to the downlake end.

(4) The sediment discharge from a mouth of en-glacial tunnels induces sediment-laden underflows and relatively clear downward compensation currents, which controls the thermal structure below the pycnocline through the transport of suspension. The relatively strong stratification by SSC offers stable thermal conditions of more than 0°C on the bottom. This could contribute to the ice-melt below the lake bottom by weak or nearly molecular heat diffusion in the lake and heat conductivity in the debris-water mixture and the upper sediment-water media.

The glacier ice below the bottom is probably distributed massively. In order to estimate the rate of the bottom subsidence, therefore, it is necessary to know the thicknesses of lake sediment and the lower debris-water mixture. These thicknesses could be estimated by means of the seismic profiling for the sedimentary structure or from the present sedimentation rate and aerial debris cover on the glacier.

Acknowledgments

We are very grateful to Dr. G.R. Bhatta, Executive Secretary of Water and Energy Commission Secretariat (WECS), Ministry of Water Resources, Nepal, for his cooperation for the field survey and research. We are also indebted to Mr. K.P. Rizal, the head of GLOF Unit for the helpful preparation of the field survey. This study was made as a GLOF (Glacier Lake Outburst Flood) research program assisted by Japan International Cooperation Agency (JICA).

References

Chikita, K.A., N.D. Smith, N. Yonemitsu and M. Perez-Arlucea, 1996. Dynamics of sediment-laden underflows passing over a subaqueous sill: glacier-fed Peyto Lake, Alberta, Canada. Sedimentology, **43**, 865-875.

Chikita, K., T. Yamada, A. Sakai, R.P. Ghimire and T. Kadota, 1996. The basin extension and outburst potentiality of a supraglacial lake in the Nepal Himalaya: A reconnaissance study. Geophys. Bull. of Hokkaido Univ., **59**, 39-50 (in Japanese with English

abstract).

Chikita, K., T. Yamada, A. Sakai and R.P. Ghimire, 1997. Hydrodynamic effects on the basin expansion of Tsho Rolpa Glacier Lake in the Nepal Himalaya. Bull. Glacier Res., **15**, 59-69.

Chikita, K. , N. Yonemitsu and Y. Yoshida, 1991. Dynamic sedimentation processes in a glacier-fed lake, Peyto Lake, Alberta, Canada. Jpn. Jour. Limnol., **52**, 27-43.

Hamblin, P.F. and E.C. Carmack, 1978. River-induced currents in a fjord lake. Jour. Geophys. Res., **83**, 885-899.

Kadota, T., 1994. Report for the field investigation on the Tsho Rolpa glacier lake, Rolwaling valley, February 1993-June 1994, WECS N551.489 KAD.

Mool, K., T. Kadota, P.R. Maskey, S. Pokharel and S. Joshi, 1993. Interim report on the field investigation on the Tsho Rolpa glacier lake, Rolwaling valley. WECS Report No. 3/4/0121193/1/1, Seq. No. 436.

Sakai, A., 1995. Thermal characteristics of the Tsho Rolpa glacier lake. M. Sc. Thesis, Hokkaido University, 66 pp (in Japanese).

Yamada, T., 1993. *Glacier lakes and their outburst floods in the Nepal Himalayas.* WECS/JICA, 37 pp.

Yamada, T., 1996. *Report on the investigations of Tsho Rolpa Glacier Lake, Rolwaling Valley.* WECS/JICA, 129 pp.